Research Article

Md Faisal Md Basir, Kohilavani Naganthran, Ehtsham Azhar, Zaffar Mehmood,
Swati Mukhopadhyay, Roslinda Nazar, Anuar Jamaludin, Dumitru Baleanu,
Kottakkaran Sooppy Nisar, and Ilyas Khan*

Unsteady nano-bioconvective channel flow with effect of nth order chemical reaction

Abstract: Nanofluid bioconvective channel flow is an essential aspect of the recent healthcare industry applications, such as biomedical processing systems. Thus, the present work examined the influence of nth order chemical reaction in an unsteady nanofluid bioconvective channel flow in a horizontal microchannel with expanding/contracting walls. The suitable form of the similarity transformation is exercised to transform the governing boundary layer equations into a more straightforward form of system to ease the computation process. The Runge–Kutta method of fifth-order integration technique solved the reduced boundary layer system and generated the numerical results as the governing parameters vary. It is found that the destructive second-order chemical reaction enhances the mass transfer rate at the lower wall but deteriorates the mass transfer rate at the upper wall. The upper channel wall has a better heat transfer rate than the lower wall when the Reynolds number increases.

* **Corresponding author: Ilyas Khan,** Faculty of Mathematics and Statistics, Ton Duc Thang University, Ho Chi Minh City, 72915, Vietnam, e-mail: ilyaskhan@tdtu.edu.vn

Md Faisal Md Basir: Department of Mathematical Sciences, Faculty of Science, Universiti Teknologi Malaysia, Skudai, Johor Bahru, 81310, Malaysia, e-mail: mfaisalmbasir@utm.my

Kohilavani Naganthran: Department of Mathematical Sciences, Faculty of Science and Technology, Universiti Kebangsaan Malaysia, UKM Bangi, 43600 Selangor, Malaysia, e-mail: kohi@ukm.edu.my

Ehtsham Azhar: Department of Information Technology, PMAS ARID Agriculture University, Rawalpindi, Pakistan, e-mail: ehtsham@uaar.edu.pk

Zaffar Mehmood: Department of Information Technology, PMAS ARID Agriculture University, Rawalpindi, Pakistan, e-mail: zaffarilyas@gmail.com

Swati Mukhopadhyay: Department of Mathematics, The University of Burdwan, Burdwan-713104, W.B., India, e-mail: swati_bumath@yahoo.co.in

Roslinda Nazar: Department of Mathematical Sciences, Faculty of Science and Technology, Universiti Kebangsaan Malaysia, UKM Bangi, 43600 Selangor, Malaysia, e-mail: rmn@ukm.edu.my

Anuar Jamaludin: Department of Mathematics, Universiti Pertahanan Nasional Malaysia, Kuala Lumpur, 57000, Malaysia, e-mail: mohdanuar@upnm.edu.my

Dumitru Baleanu: Department of Mathematics, Cankaya University, Ankara, Turkey; Institute of Space Sciences, Magurele, 077125, Romania; Department of Medical Research, China Medical University Hospital, China Medical University, Taichung, Taiwan, e-mail: Baleanu@mail.cmuh.org.tw

Kottakkaran Sooppy Nisar: Department of Mathematics, College of Arts and Sciences, Prince Sattam bin Abdulaziz University, Wadi Aldawaser, 11991, Saudi Arabia, e-mail: n.sooppy@psau.edu.sa

Nomenclature

a	length of the channel (m)
$\dot{a}$	time-dependent rate (m/s)
A	injection coefficient (−)
$\tilde{b}$	chemotaxis constant (m)
C	nanoparticle volume fraction (−)
C_0	reference nanoparticle volume fraction (−)
C_1	nanoparticle volume fraction on lower wall (−)
C_2	nanoparticle volume fraction on upper wall (−)
c_{p}	specific heat at constant pressure (J/kg/K)
D_{B}	Brownian diffusion coefficient (m²/s)
D_{n}	variable microorganism diffusion coefficient (m²/s)
D_{T}	thermophoretic diffusion coefficient
$f(\eta)$	dimensionless stream function (−)
$\overrightarrow{j}$	vector flux of microorganisms (kg/m²/s)
k	thermal conductivity (W/mK)
k_1	rate of chemical reaction (1/s)
K_{r}	chemical reaction parameter (−)
Lb	bioconvection Lewis number $\left(\mathrm{Lb} = \frac{\alpha_0}{D_{\mathrm{n}}}\right)$ (−)
Le	Lewis number $\left(\mathrm{Le} = \frac{\alpha_0}{D_{\mathrm{B}}}\right)$ (−)
Nb	Brownian motion parameter $\left(\mathrm{Nb} = \frac{\tau D_{\mathrm{B}}(C_2 - C_0)}{\alpha_0}\right)$ (−)

Nt	thermophoresis parameter ($Nt = \frac{\tau D_T (T_2 - T_0)}{\alpha_0 T_0}$) $(-)$
N	number of motile microorganisms $(-)$
N_1	lower wall motile microorganisms $(-)$
N_2	upper wall motile microorganisms $(-)$
n	power-law index
p	pressure (N/m^2) $(-)$
Pe	bioconvection Péclet number $\left(Pe = \frac{\tilde{b} W_c}{D_n} \right)$ $(-)$
Pr	Prandtl number $\left(Pr = \frac{\upsilon}{\alpha_0} \right)$ $(-)$
Re	Reynolds number $\left(\frac{a \upsilon_w}{\upsilon} \right)$ $(-)$
$\bar{t}$	dimensional time (s)
T	temperature (K)
T_0	reference temperature (K)
T_1	temperature at the lower wall (K)
T_2	temperature at the upper wall (K)
$\bar{u}$	velocity components along the $\bar{x}$-axis (m/s)
$\overrightarrow{v}$	velocity vector (m/s)
$\overrightarrow{\hat{v}}$	average swimming velocity vector of micro-organism (m^2/s)
$\bar{v}$	velocity components along the $\bar{y}$-axis (m/s)
$\bar{v}_w$	dimensional inflow/outflow velocity (m/s)
W_c	maximum cell swimming speed (m/s)
$\bar{x}$	dimensional coordinate along the surface (m)
$\bar{y}$	coordinate normal to the surface (m)

Greek letters

α_0	effective thermal diffusivity (m^2/s)
α	wall expansion ratio $(-)$
η	independent similarity variable $(-)$
$\theta(\eta)$	dimensionless temperature $(-)$
θ_1	constant $(-)$
μ	dynamic viscosity (kg/m/s)
υ	kinematic viscosity (m^2/s)
ρ	fluid density (kg/m^3)
$(\rho c)_f$	volumetric heat capacity of the fluid (J/m^3/K)
$(\rho c)_p$	volumetric heat capacity of the nanoparticle material (J/m^3/K)
τ	ratio of the effective heat capacity of the nanoparticle material to the fluid heat capacity $\left(\frac{(\rho c)_p}{(\rho c)_f} \right)$ $(-)$
$\phi(\eta)$	dimensionless nanoparticles volume fraction $(-)$
ϕ_1	constant $(-)$
$\chi(\eta)$	dimensionless number of motile microorganisms $(-)$
χ_1	constant $(-)$

Subscripts

$(\ )'$	ordinary differentiation with respect to η
$(\ )_0$	condition at reference
$(\ )_1$	condition at lower wall
$(\ )_2$	condition at upper wall

1 Introduction

Nanofluids find applications in many fields of science and engineering that require heat transfer fluids [1,2]. Generally, conventional heat transfer fluids are poor heat transfer fluids as their thermal conductivity is very low [3]. Metals have superior thermal conductivity compared to usual heat transfer fluids. Therefore, a "technique" has been developed for the enhancement of the thermal conductivity of the base fluids by incorporating nano/micro-sized metallic particles in liquids. A suitable method to increase the heat transfer coefficient is via the suspension of ultrafine solid metallic particles in industrial fluids [4]. Nanofluid is the composition of subatomic particles in the base fluid, with a dimension of order 10^{-9}, which plays a remarkable role in improving the thermal conductivity and convective heat transfer [5]. Usually, these particles (called nanoparticles) are oxides of metals, pure metallic particles, or even carbon nanotubes [6]. Nanofluid formation is possible through different combinations of base fluid and nanoparticles. Many models have been developed by scientists to account for how much the thermal conductivity increase would be, and many experiments have been carried out to compare experimental data with results of analytical models. In modelling nanofluid flows, generally, two approaches (single-phase model and two-phase model) are used. When nanoparticles are dropped in the base fluid that is very small (less than 10 nm) in size, the nanoparticles easily fluidize, and as a result, nanoparticles are uniformly dispersed and suspended stably in the base fluid. Consequently, the solid particles and the fluid both remain in the same phase and behave as a homogeneous fluid. On the other hand, some nanofluid models have been proposed to assist the researchers to investigate the nanofluid phenomena. Khanafer et al. [7] have proposed a nanofluid model, which is assumed to be in a single phase, achieves thermal equilibrium and omits velocity slip between base fluid and particle. However, the nanofluid model of Khanafer et al. [7] disregarded some crucial factors such as size, shape and distribution of the particle and focused on investigating the dispersion effect. Then,

Tiwari and Das [8] came up with a simpler nanofluid single-phase model than the model introduced by Khanafer et al. [7], which is known as the Tiwari and Das model. Meanwhile, Buongiorno [9] presented another nanofluid model to improvise those homogenous single-phase and thermal dispersion models by defining the base fluid effect and the nanoparticle's relative velocity more mechanically than in the thermal dispersion model proposed by Khanafer et al. [7]. Buongiorno [9] pointed out that Brownian motion and thermophoresis were the primary sources for heat transfer improvement in nanofluids. These are the recent literature depicting the flow of nanofluids/hybrid nanofluids on a moving surface with several effects (see ref. [10–14]).

Bioconvection is a result of an unbalanced density stratification that is caused by up-swimming microorganisms [15]. The unbalanced density stratification happens as soon as the microorganisms accumulate at the top of the fluid [16]. There are two useful types of up-swimming microorganisms, frequently utilized in bioconvection experiments, namely, stable oxytactic bacteria and bottom-heavy algae [1]. Bioconvection usually occurs with smaller nanoparticle concentration (≤1%). Consequently, the viscosity of the base fluid remains unaltered. For practical purposes, it is necessary to understand the character of suspensions containing both nanoparticles and self-swimming microorganisms in microsystems. Enhancement of mass transportation ability and mixing and reduction in the sedimentation of species are among the applications of bioconvection in bio-microsystems and the pharmaceutical industries [1,17–19]. Nanofluids, together with bioconvection, termed nano-bioconvection, are helpful to attain improved thermal performance as well as green, sustainable features. This makes them well-suited to be used as next-generation bio-fuels [16]. In geophysical phenomena, thermo-bioconvection (with heat-loving microorganisms) plays a key role in hot spring areas [20]. It can also be applied to microbial enhanced oil recovery field; in this industry, microorganisms and nutrients are exploited by mounting them in oil-bearing glaciers to adjust a permeability variation. Uddin et al. [21] reported the effects of bioconvection parameters on the flow of a nanofluid full of suspended gyrotactic microorganisms. Various researchers, see ref. [22–26], have investigated the nano-bioconvective flow for Newtonian as well as non-Newtonian fluids.

Chemical reaction plays an essential part in certain applications involving heat and mass transport [27]. Chemical reactions may be considered as either homogenous or heterogeneous chemical reactions. All the reactants are in the same phase in the case of homogeneous reactions, while in heterogeneous reactions the reactants are in two or more phases. A reaction is said to be of order n if the rate of reaction is directly proportional to the nth power of species concentration. The concentration difference is the primary motivating force for mass transfer [28]. Moreover, fluid flow through a channel made of two porous parallel plates has attracted significant interest in the last few years [29]. The fluid flow through extending/contracting walls has been applied in biophysical flows such as respiratory system, dialysis, filtration in tissues and oxygen diffusion in capillaries [30]. Due to its vast applications, several researchers, such as Ahmed et al. [31], Darvishi et al. [32], Javanmard et al. [33], Mosayebidorcheh [34] and Odelu and Kumar [35], considered many multi-physical effects on the channel flow between the extending/contracting walls.

With this regard, in the present work, we expanded the analysis of a study conducted by Xinhui et al. [36] and Bég et al. [30] in that we take into consideration the nth order chemical reaction. The channel consists of the expanding/contracting upper and lower walls, which are parallel and permeable. The Runge–Kutta fifth-order method associated with the shooting technique has been employed to produce numerical solutions. To the best of the authors' knowledge, all presented results on the present model are novel.

2 Mathematical model

Figure 1 illustrates a two-dimensional view of unsteady laminar forced bioconvective slip flow of a nanofluid in a horizontal semi-infinite channel. The distance between the two walls is $\bar{a}(\bar{t})$. The upper wall and lower wall of the channel are subjected to wall velocity, $\bar{v}_w$, and it is expanding or uniformly contracting at a time-dependent rate, $\frac{\partial \bar{a}}{\partial \bar{t}}$. Consequently, the plate separation is a function of time and equals $\bar{a}(\bar{t})$

The following assumptions are made:
- Nanoparticle suspension is stable and does not allow agglomeration in the fluid.
- Water-based nanofluid with the presence of gyrotactic microorganisms is considered.
- Unsteady two-dimensional incompressible flow.
- Nanoparticles independent of the direction of micro-organisms swimming.
- Water is considered as the base fluid and spherical (or close to spherical)-shaped nanoparticles are chosen in the present study. $\bar{u}$ and $\bar{v}$ refer to the velocity components in both $\bar{x}$ and $\bar{y}$ directions. T, C and N denote the

fluid temperature, nanoparticle volume fraction and motile microorganism density, respectively. The lower wall temperature is symbolized by T_1 while T_2 is the upper wall temperature. Next, the nanoparticle volume fractions at the lower and upper walls are given as C_1 and C_2, respectively. The densities of motile microorganisms at the lower and upper walls are indicated by N_1 and N_2, respectively. Based on these assumptions and the reliability of Buongiorno's model, the governing boundary layer equations of mass, momentum, thermal energy, nano-particle concentration and microorganism density conservation are stated as follows [37]:

$$\nabla \cdot \vec{v} = 0, \tag{1}$$

$$\frac{\partial \vec{v}}{\partial \bar{t}} + (\vec{v} \cdot \nabla) \vec{v} = -\frac{1}{\rho} \nabla p + \upsilon \nabla^2 \vec{v}, \tag{2}$$

$$\frac{\partial T}{\partial \bar{t}} + (\vec{v} \cdot \nabla) T$$
$$= \alpha_0 \nabla^2 T + \tau \left[D_B \nabla T \cdot \nabla C + \left(\frac{D_T}{T_0} \right) \nabla T \cdot \nabla T \right], \tag{3}$$

$$\frac{\partial C}{\partial \bar{t}} + (\vec{v} \cdot \nabla) C$$
$$= D_B \nabla^2 C + \tau \left[\left(\frac{D_T}{T_0} \right) \nabla^2 T \right] - k_1 (C - C_0)^n, \tag{4}$$

$$\frac{\partial N}{\partial \bar{t}} + \nabla \cdot \vec{j} = 0, \tag{5}$$

where $\vec{v} = (\bar{u}, \bar{v})$ are the velocity components along x and y axes, respectively. $\nabla = \frac{\partial}{\partial x} \vec{i} + \frac{\partial}{\partial y} \vec{j}$ is the del or gradient operator, $\nabla^2 = \frac{\partial^2}{\partial x^2} \vec{i} + \frac{\partial^2}{\partial y^2} \vec{j}$ is the Laplacian operator, p is the pressure, $\tau = \frac{(\rho c)_p}{(\rho c)_f}$ is the ratio of nanoparticle heat capacity and the base fluid heat capacity, $\alpha_0 = \frac{k}{(\rho c)_f}$ is the thermal diffusivity of the fluid, ρ is the density of the base fluid, υ is the kinematic viscosity, D_B is the

Figure 1: A schematic diagram of the physical flow problem (Hatami et al. [29]).

Brownian diffusion coefficient, D_T is the thermophoresis diffusion coefficient, T_0 is the reference temperature, C_0 is the reference concentration, k_1 is the rate of chemical reaction and n is the concentration power law index.

Furthermore, $\vec{j}$ represents the flux of microorganisms and can be written as follows:

$$\vec{j} = N \vec{v} + N \hat{v} - D_n \nabla^2 N. \tag{6}$$

Also, $\hat{v} = \left(\frac{\tilde{b} W_c}{C_1 - C_0} \right) \nabla C$ is the average swimming velocity vector of microorganisms in nanofluids, D_n is the species diffusivity of microorganisms, $\tilde{b}$ is the chemotaxis constant and W_c is the maximum cell swimming speed.

Now, for the two-dimensional nano-bioconvection case, equations (1)–(5) can be written as:

$$\frac{\partial \bar{u}}{\partial \bar{x}} + \frac{\partial \bar{v}}{\partial \bar{y}} = 0, \tag{7}$$

$$\frac{\partial \bar{u}}{\partial \bar{t}} + \bar{u} \frac{\partial \bar{u}}{\partial \bar{x}} + \bar{v} \frac{\partial \bar{u}}{\partial \bar{y}} = -\frac{1}{\rho} \frac{\partial p}{\partial \bar{x}} + \upsilon \left(\frac{\partial^2 \bar{u}}{\partial \bar{x}^2} + \frac{\partial^2 \bar{u}}{\partial \bar{y}^2} \right), \tag{8}$$

$$\frac{\partial \bar{v}}{\partial \bar{t}} + \bar{u} \frac{\partial \bar{v}}{\partial \bar{x}} + \bar{v} \frac{\partial \bar{u}}{\partial \bar{y}} = -\frac{1}{\rho} \frac{\partial p}{\partial \bar{y}} + \upsilon \left(\frac{\partial^2 \bar{v}}{\partial \bar{x}^2} + \frac{\partial^2 \bar{v}}{\partial \bar{y}^2} \right), \tag{9}$$

$$\frac{\partial T}{\partial \bar{t}} + \bar{u} \frac{\partial T}{\partial \bar{x}} + \bar{v} \frac{\partial T}{\partial \bar{y}}$$
$$= \alpha_0 \left(\frac{\partial^2 T}{\partial x^2} + \frac{\partial^2 T}{\partial \bar{y}^2} \right)$$
$$+ \tau \left[D_B \left(\frac{\partial T}{\partial \bar{x}} \frac{\partial C}{\partial \bar{x}} + \frac{\partial T}{\partial \bar{y}} \frac{\partial C}{\partial \bar{y}} \right) + \frac{D_T}{T_0} \left[\left(\frac{\partial T}{\partial \bar{x}} \right)^2 + \left(\frac{\partial T}{\partial \bar{y}} \right)^2 \right] \right], \tag{10}$$

$$\frac{\partial C}{\partial \bar{t}} + \bar{u} \frac{\partial C}{\partial \bar{x}} + \bar{v} \frac{\partial C}{\partial \bar{y}}$$
$$= D_B \left(\frac{\partial^2 C}{\partial \bar{x}^2} + \frac{\partial^2 C}{\partial \bar{y}^2} \right) \tag{11}$$
$$+ \frac{D_T}{T_0} \left(\frac{\partial^2 T}{\partial \bar{x}^2} + \frac{\partial^2 T}{\partial \bar{y}^2} \right) - k_1 (C - C_0)^n,$$

$$\frac{\partial N}{\partial \bar{t}} + \bar{u} \frac{\partial N}{\partial \bar{x}} + \bar{v} \frac{\partial N}{\partial \bar{y}} + \frac{\tilde{b} W_c}{C_1 - C_0}$$
$$\left[\frac{\partial}{\partial \bar{x}} \left(N \frac{\partial C}{\partial \bar{x}} \right) + \frac{\partial}{\partial \bar{y}} \left(N \frac{\partial C}{\partial \bar{y}} \right) \right] = D_n \left(\frac{\partial^2 N}{\partial \bar{x}^2} + \frac{\partial^2 N}{\partial \bar{y}^2} \right). \tag{12}$$

The relevant boundary conditions are given as follows:

$$\begin{aligned} \bar{u} = 0, \ \bar{v} = \bar{v}_w = A\dot{\bar{a}}(\bar{t}), \\ T = T_1, C = C_1, N = N_1 \quad \text{at } \bar{y} = -\bar{a}(\bar{t}), \\ \bar{u} = 0, \ \bar{v} = -\bar{v}_w = -A\dot{\bar{a}}(\bar{t}), \\ T = T_2, C = C_2, N = N_2 \quad \text{at } \bar{y} = \bar{a}(\bar{t}), \end{aligned} \tag{13}$$
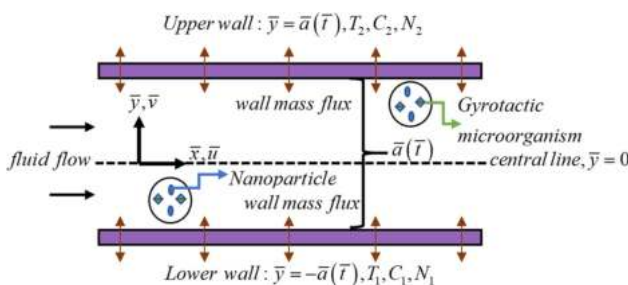
where $A = \bar{v}_{\mathrm{w}}/\dot{\bar{a}}(\bar{t})$ refers to the injection coefficient; it is a wall measure of permeability. The following similarity transformations are specified:

$$\psi = \frac{\upsilon \bar{x}}{\bar{a}(\bar{t})} F(\eta, \bar{t}),$$

$$\eta = \frac{\bar{y}}{\bar{a}(\bar{t})},$$

$$\bar{u} = \frac{\upsilon}{\bar{a}^2(\bar{t})} \bar{x} F'(\eta, \bar{t}), \bar{v} = \frac{-\upsilon}{\bar{a}(\bar{t})} F(\eta, \bar{t}), \quad (14)$$

$$\theta(\eta) = \frac{T - T_0}{T_1 - T_0}, \quad \phi(\eta) = \frac{C - C_0}{C_1 - C_0}, \quad \chi(\eta) = \frac{N}{N_1}.$$

Equation (14) is substituted into equations (7)–(12) jointly with boundary conditions (13). The pressure gradient terms are eliminated from the momentum equations (8) and (9). Consequently, the system of similarity differential equations concerning space and time can be attained:

$$f^{(\mathrm{iv})} + \mathrm{Re}(ff''' - f'f'') + \alpha(\eta f''' + 3f'') = 0, \quad (15)$$

$$\theta'' + \mathrm{Pr}\,\mathrm{Re}\,f\theta' + \mathrm{Nb}\phi'\theta' + \mathrm{Nt}\theta'^2 + \mathrm{Pr}\alpha\eta\theta' = 0, \quad (16)$$

$$\phi'' + \mathrm{PrLe}\,\mathrm{Re}\,f\phi' + \frac{\mathrm{Nt}}{\mathrm{Nb}}\theta'' + \mathrm{PrLe}\alpha\eta\phi' - K_r\phi^n = 0, (17)$$

$$\chi'' - \mathrm{Pe}(\phi'\chi' + \chi\phi'') + \mathrm{LbPr}\,\mathrm{Re}\,f\chi' + \mathrm{LbPr}\alpha\eta\chi' = 0, (18)$$

where $f = \frac{F}{\mathrm{Re}}$, $\mathrm{Re} = \frac{\bar{a}\bar{v}_{\mathrm{w}}}{\upsilon}$ is the Reynolds number, $\alpha = \frac{\bar{a}\dot{\bar{a}}}{\upsilon}$ is the wall expansion ratio, $\mathrm{Pr} = \frac{\upsilon}{\alpha_0}$ is the Prandtl number, $\mathrm{Nb} = \frac{\tau D_{\mathrm{B}}(C_1 - C_0)}{\alpha_0}$ is the Brownian motion parameter, $\mathrm{Nt} = \frac{\tau D_{\mathrm{T}}(T_1 - T_0)}{\alpha_0 T_0}$ is the thermophoresis parameter, $\mathrm{Le} = \frac{\alpha_0}{D_{\mathrm{B}}}$ is the Lewis number, $K_r = \frac{k_1 \bar{a}^2 (C_1 - C_0)^{n-1}}{\upsilon}$ is the chemical reaction parameter, $\mathrm{Lb} = \frac{\alpha_0}{D_{\mathrm{n}}}$ is the bioconvection Lewis number and $\mathrm{Pe} = \frac{\bar{b}W_{\mathrm{c}}}{D_{\mathrm{n}}}$ is the bioconvection Péclet number.

It is worth noting that $\alpha < 0$ corresponds to a contracting wall and on the other hand $\alpha > 0$ corresponds to an expanding wall. If $\alpha = 0$, it means the wall is static i.e. fixed channel plate separation. The corresponding boundary conditions are as follows:

$$f(-1) = -1, f'(-1) = 0, \theta(-1) = 1, \phi(-1) = 1, \chi(-1) = 1, \quad (19)$$
$$f(1) = 1, f'(1) = 0, \theta(1) = \theta_1, \phi(1) = \phi_1, \chi(1) = \chi_1,$$

where $\theta_1 = \frac{T_2 - T_0}{T_1 - T_0}, \phi_1 = \frac{C_2 - C_0}{C_1 - C_0}, \chi_1 = \frac{N_2}{N_1}$ are constants. In this study, we restrain to the positive values of the Reynolds number $\mathrm{Re} \geq 0$. It physically corresponds to injection at the upper/lower wall.

As far as the practical interest quantities are concerned, they are introduced as the skin friction coefficient ($C_{f\bar{x}}$), the local Nusselt number ($\mathrm{Nu}_{\bar{x}}$), the local Sherwood number ($\mathrm{Sh}_{\bar{x}}$), the local density numbers of motile microorganisms ($\mathrm{Nn}_{\bar{x}}$), the wall skin friction (τ_{w}), the wall heat flux (q_{w}), the wall mass flux (q_{m}) and the microorganism flux (q_{n}), which can be defined as follows:

At the lower wall:

$$C_{f\bar{x}} = \frac{2\tau_{\mathrm{w}}}{\rho_f U_{\mathrm{R}}^2}, \quad \mathrm{Nu}_{\bar{x}} = \frac{-\bar{a}(\bar{t})q_{\mathrm{w}}}{k(T_1 - T_0)},$$
$$\mathrm{Sh}_{\bar{x}} = \frac{-\bar{a}(\bar{t})q_{\mathrm{m}}}{D_{\mathrm{B}}(C_1 - C_0)}, \quad \mathrm{Nn}_{\bar{x}} = \frac{-\bar{a}(\bar{t})q_{\mathrm{n}}}{D_{\mathrm{n}}N_1}, \quad (20)$$

where

$$\tau_{\mathrm{w}} = \mu\left(\frac{\partial u}{\partial \bar{y}}\right)_{\bar{y}=\bar{a}(\bar{t})}, \quad q_{\mathrm{w}} = -k\left(\frac{\partial T}{\partial \bar{y}}\right)_{\bar{y}=\bar{a}(\bar{t})},$$
$$q_{\mathrm{m}} = -D_{\mathrm{B}}\left(\frac{\partial C}{\partial \bar{y}}\right)_{\bar{y}=\bar{a}(\bar{t})}, \quad q_{\mathrm{n}} = -D_{\mathrm{n}}\left(\frac{\partial N}{\partial \bar{y}}\right)_{\bar{y}=\bar{a}(\bar{t})}. \quad (21)$$

At the upper wall:

$$C_{f\bar{x}} = \frac{2\tau_{\mathrm{w}}}{\rho_f U_{\mathrm{R}}^2}, \quad \mathrm{Nu}_{\bar{x}} = \frac{-\bar{a}(\bar{t})q_{\mathrm{w}}}{k(T_2 - T_0)},$$
$$\mathrm{Sh}_{\bar{x}} = \frac{-\bar{a}(\bar{t})q_{\mathrm{m}}}{D_{\mathrm{B}}(C_2 - C_0)}, \quad \mathrm{Nn}_{\bar{x}} = \frac{-\bar{a}(\bar{t})q_{\mathrm{n}}}{D_{\mathrm{n}}N_2}, \quad (22)$$

where

$$\tau_{\mathrm{w}} = \mu\left(\frac{\partial u}{\partial \bar{y}}\right)_{\bar{y}=\bar{a}(\bar{t})}, \quad q_{\mathrm{w}} = -k\left(\frac{\partial T}{\partial \bar{y}}\right)_{\bar{y}=-\bar{a}(\bar{t})},$$
$$q_{\mathrm{m}} = -D_B\left(\frac{\partial C}{\partial \bar{y}}\right)_{\bar{y}=-\bar{a}(\bar{t})}, \quad q_{\mathrm{n}} = -D_{\mathrm{n}}\left(\frac{\partial N}{\partial \bar{y}}\right)_{\bar{y}=-\bar{a}(\bar{t})}. \quad (23)$$

Here, U_{R} is the average channel flow velocity and μ is the dynamic viscosity. By substituting equations (14), (21) and (23) into equations (20) and (22), the resulting expressions are as follows:

$$C_{f\bar{x}} = \frac{1}{\mathrm{Re}^2}f''(-1), \quad \mathrm{Nu}_{\bar{x}} = -\theta'(-1),$$
$$\mathrm{Sh}_{\bar{x}} = -\phi'(-1), \quad \mathrm{Nn}_{\bar{x}} = -\chi'(-1),$$
$$C_{f\bar{x}} = \frac{1}{\mathrm{Re}^2}f''(1), \quad \mathrm{Nu}_{\bar{x}} = -\frac{\theta'}{\theta_1}(-1), \quad (24)$$
$$\mathrm{Sh}_{\bar{x}} = -\frac{\phi'}{\phi_1}(-1), \quad \mathrm{Nn}_{\bar{x}} = -\frac{\chi'}{\chi_1}(-1).$$

Calculating the skin friction is beneficial in approximating total frictional drag exerted on a solid surface. At the same time, the local Nusselt number and the local Sherwood number are essential for estimating the convective heat transfer rate and mass transfer rate on a solid surface.

3 Numerical solution and validation

Equations (15)–(18) under boundary conditions (19) define strongly nonlinear two-point boundary problems. Thus, a computational method, namely, the Runge–Kutta fifth-order method associated with the shooting technique, is implemented. These coupled nonlinear differential equations are converted into a system of first-order ordinary differential equations and then are transformed into initial value problem with variables labelled as:

$$
\begin{pmatrix} f \\ f' \\ f'' \\ f''' \\ \theta \\ \theta' \\ \phi \\ \phi' \\ \chi \\ \chi' \end{pmatrix} = \begin{pmatrix} y_1 \\ y_1' = y_2 \\ y_2' = y_3 \\ y_3' = y_4 \\ y_5 \\ y_5' = y_6 \\ y_7 \\ y_7' = y_8 \\ y_9 \\ y_9' = y_{10} \end{pmatrix}. \tag{25}
$$

The system of equations can be formulated as follows:

$$
\begin{pmatrix} y_1' \\ y_2' \\ y_3' \\ y_4' \\ y_5' \\ y_6' \\ y_7' \\ y_8' \\ y_9' \\ y_{10}' \end{pmatrix} = \begin{pmatrix} y_2 \\ y_3 \\ y_4 \\ -Re(y_1 y_4 - y_2 y_3) - \alpha(\eta y_4 + 3y_3) \\ y_6 \\ -Pr\,Re\,y_1 y_6 - Nb y_6 y_8 - Nt y_6^2 - Pr\alpha\eta y_6 \\ y_8 \\ -PrLe\,Re\,y_1 y_8 - \dfrac{Nt}{Nb}y_6' - PrLe\alpha\eta y_8 + Kr y_7^n \\ y_{10} \\ Pe(y_8 y_{10} + y_9 y_8') - LbPr\,Re\,y_1 y_{10} - LbPr\alpha\eta y_{10} \end{pmatrix} \tag{26}
$$

$$
\begin{pmatrix} y_1(-1) \\ y_2(-1) \\ y_3(-1) \\ y_4(-1) \\ y_5(-1) \\ y_6(-1) \\ y_7(-1) \\ y_8(-1) \\ y_9(-1) \\ y_{10}(-1) \end{pmatrix} = \begin{pmatrix} -1 \\ 0 \\ S_1 \\ S_2 \\ 1 \\ S_3 \\ 1 \\ S_4 \\ 1 \\ S_5 \end{pmatrix}. \tag{27}
$$

The above initial value problem can be solved by implementing the Runge–Kutta method of order 5 integration, and S_1, S_2, S_3, S_4 and S_5 represent the appropriate

values of unknown initial conditions. They are estimated by putting Newton's method to a test until boundary conditions of $f(\eta) \to 1$, $f'(\eta) \to 0$, $\theta(\eta) \to \theta_1$, $\phi(\eta) \to \phi_1$ and $\chi(\eta) \to \chi_1$ as $\eta \to 1$ are satisfied. The mathematical software MATLAB was successfully utilized for the computation purposes. End of the boundary layer region (i.e. when each group reaches $\eta = 1$) is determined as if the values of unknown boundary conditions at $y = 1$ remain unchanged to a successful loop until the far field conditions are met with respect to a specified tolerance of 10^{-6} [38].

As no data are found to compare for this specific problem, we have compared the values of f'', θ', ϕ' for some specific values of the parameters obtained by two methods (shooting and bvp4c built in function in the MATLAB) and found an excellent agreement (Table 1).

4 Results and discussion

All numerical solutions are obtained through MATLAB (RKF5 with shooting technique), and they are presented graphically for a better understanding of several aspects. The aspects are the effects of several controlling parameters on the dimensionless velocity, $f'(\eta)$, temperature $\theta(\eta)$, nanoparticle volume fraction $\phi(\eta)$ and motile microorganism density function $\chi(\eta)$. In this study, water-based bio-nanofluid has been considered and the value of $Pr = 6.8$ has been taken. MATLAB solutions are presented in Figures 3–27, whereas Figure 1 shows the flow diagram and Figure 2 presents the flow chart of
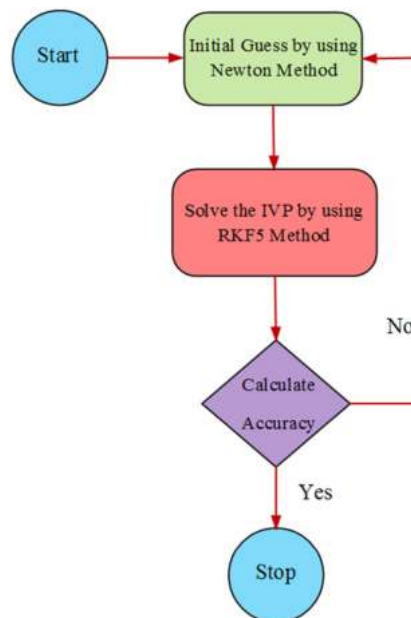

Figure 2: Flow chart of shooting method.

Table 1: Numerical values of f'', θ', ϕ' for $\alpha = 1.0$, $Nb = 0.1$, $Nt = 0.1$, $Kr = 0.1$, $Re = 2.0$, $Pe = 0.1$, $Lb = 0.1$, $Le = 1.3$, $Pr = 2.5$ and $n = 2$

η	f''		θ'		φ'	
	Shooting	bvp4c	Shooting	bvp4c	Shooting	bvp4c
−0.8	2.304949	2.30495	−0.055762	−0.0557715	−0.142846	−0.142874
−0.6	2.06599	2.06600	−0.194536	−0.194538	−0.379509	−0.379447
−0.4	1.567717	1.56773	−0.518418	−0.518346	−0.712428	−0.712474
−0.2	0.848289	0.848287	−0.984156	−0.984159	−0.878276	−0.878271
0.0	0.000001	0.00000	−1.26273	−1.26273	−0.829134	−0.82913
0.2	−0.848287	−0.848287	−1.066823	−1.06683	−0.802026	−0.802025
0.4	−1.567729	−1.56773	−0.598571	−0.598572	−0.674661	−0.674659
0.6	−2.065989	−2.06600	−0.232982	−0.232964	−0.382705	−0.382643
0.8	−2.304949	−2.30495	−0.067787	−0.0677975	−0.145767	−0.145789

shooting method. The impact of important parameters on fluid velocity $f'(\eta)$, temperature distribution $\theta(\eta)$, concentration of nanoparticles $\phi(\eta)$, and motile density of microorganisms' distribution $\chi(\eta)$ are presented and later discussed in detail.

Figures 3–27 are plotted to scrutinize the influence of pertinent parameters. The governing parameters are the Reynolds number (Re), the wall expansion ratio (α), the Prandtl number (Pr), the Brownian motion parameter (Nb), the thermophoresis parameter (Nt), the Lewis number (Le), the chemical reaction parameter (Kr), the bioconvection Lewis number (Lb) and the bioconvection Péclet number (Pe). The variations of these pertinent parameters are examined with respect to the channel wall expansion ($\alpha > 0$). Figure 3 shows the impact of the Reynolds number on $f(\eta)$. $f(\eta)$ increases at the lower wall and has an opposite effect at the upper wall. Figure 4 portrays the effect of the Reynolds number on fluid velocity, $f'(\eta)$. It is evident, as shown in Figure 4, that fluid velocity decreases as the Reynolds number increases because viscous forces become dominant when compared to inertial forces. Hence, velocity reduces and attains its maximum value for both upper and lower walls. Figure 5 displays the effects of wall expansion ratio parameter α on fluid velocity. For the lower wall expansion, there is an increase in fluid velocity; the opposite trend happens for the upper wall. An increase in velocity produces a sudden increase in yield stress and as a result increases velocity at the lower wall; vice versa, at the upper wall, an increase in yield stress leads to a resistance in the flow and finally velocity decreases. Influences of the Reynolds number on the temperature distribution $\theta(\eta)$ are shown in Figure 6. As the Reynolds number is also a ratio of inertial to viscous forces, the fluid temperature is directly affected by enhancing Re. By referring to Figure 6, the fluid temperature increases positively
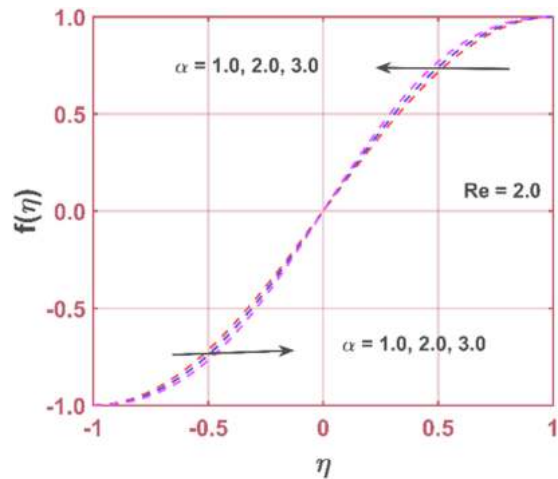
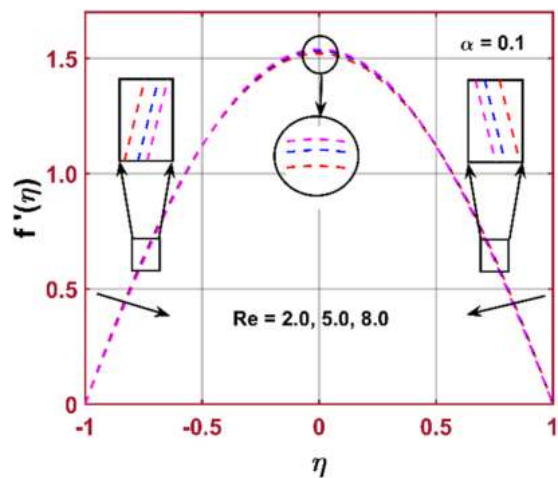

Figure 3: Effect of the wall expansion parameter (α) on $f(\eta)$.

Figure 4: Effect of the Reynolds number (Re) on $f'(\eta)$.

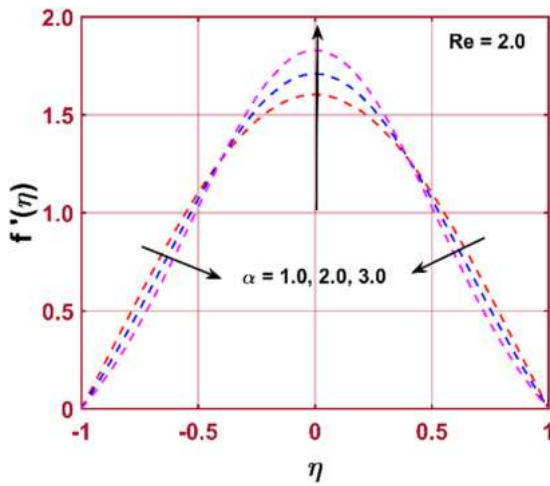**Figure 5:** Effect of the wall expansion parameter (α) on $f'(\eta)$.
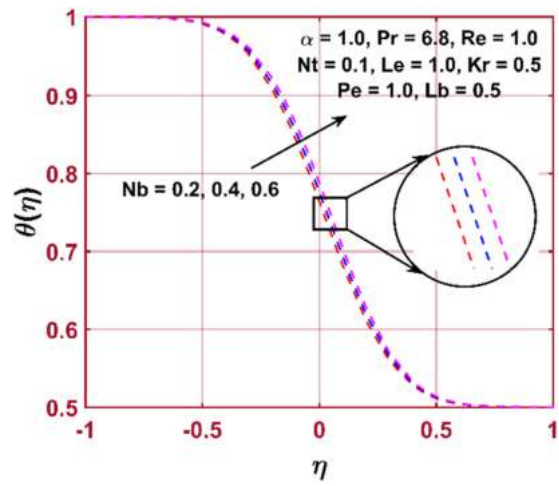

Figure 8: Effect of the Brownian parameter (Nb) on $\theta(\eta)$.
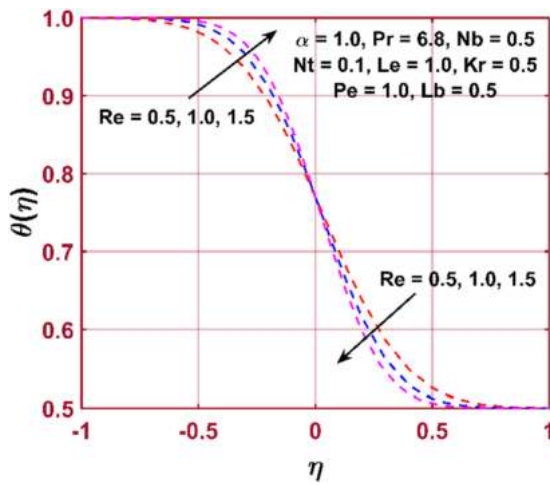

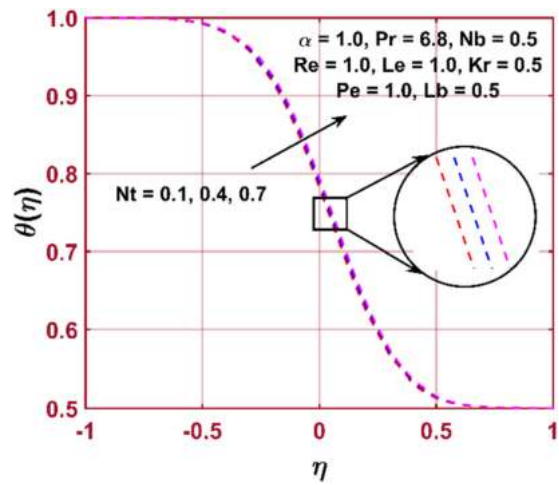**Figure 6:** Effect of the Reynolds number (Re) on $\theta(\eta)$.

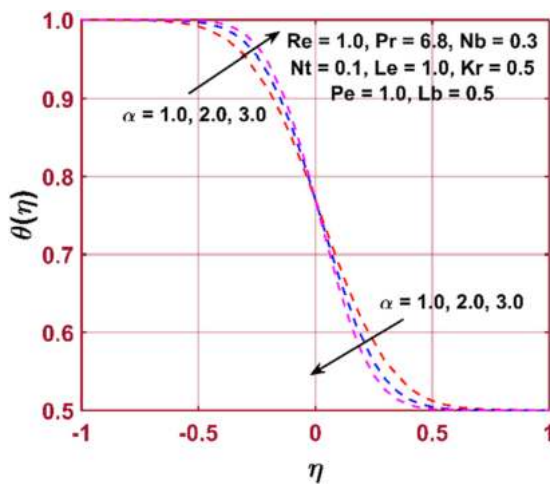**Figure 9:** Effect of the thermophoresis parameter (Nt) on $\theta(\eta)$.
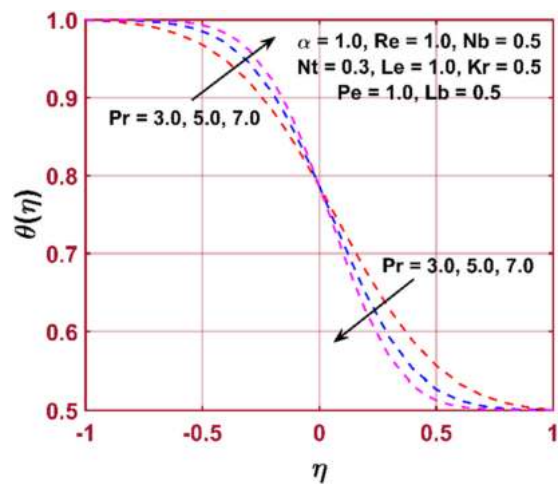

Figure 7: Effect of the wall expansion parameter α on $\theta(\eta)$.

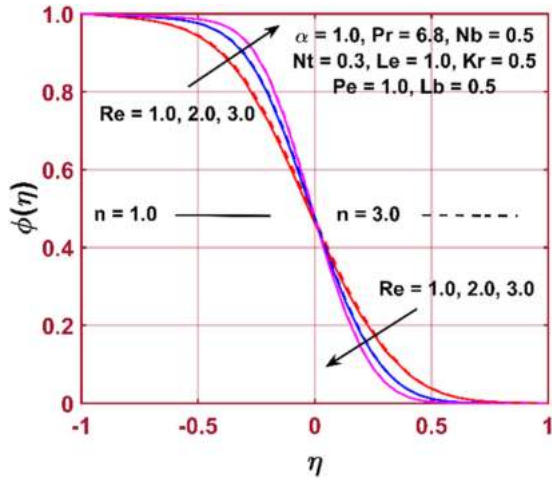**Figure 10:** Effect of the Prandtl number (Pr) on $\theta(\eta)$.

Figure 11: Effect of the Reynolds number (Re) on $\theta(\eta)$ when the power-law index is $n = 1, 3$.
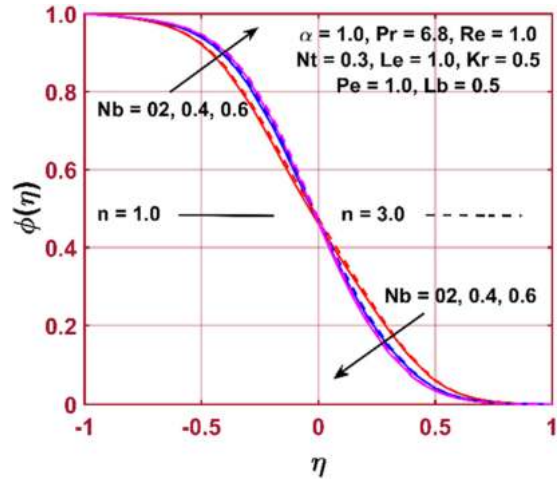
Figure 13: Effect of the Brownian parameter (Nb) on $\theta(\eta)$ when the power-law index is $n = 1, 3$.
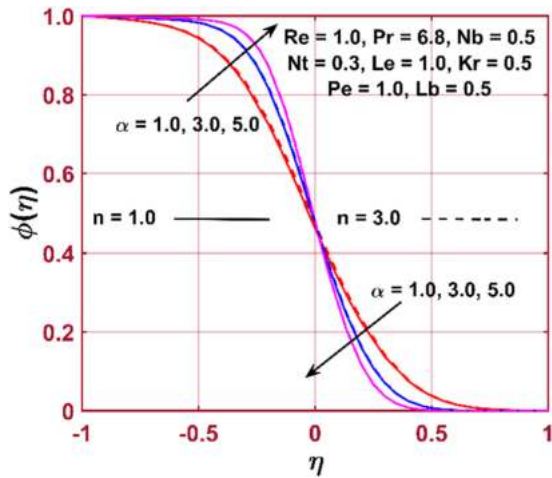
Figure 12: Effect of expansion ratio α on $\theta(\eta)$ when the power-law index is $n = 1, 3$.
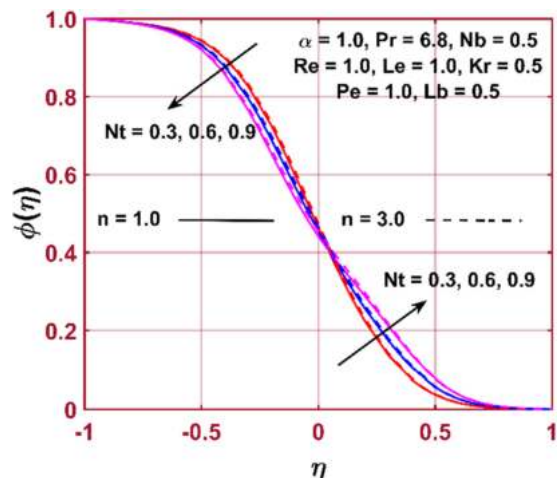
Figure 14: Effect of the thermophoresis parameter (Nt) on $\phi(\eta)$ when the power-law index is $n = 1, 3$.

with an increase in Re at the lower wall, whereas reverse behaviour is seen at the upper wall.

The effects of wall expansion parameters on temperature profile are summarized in Figure 7. Wall expansion parameter (α) increases the temperature at the lower wall, but the temperature drops down at the upper wall. Figure 8 describes the impact of Brownian parameter (Nb) for temperature distribution. The Brownian parameter results in boosting the fluid flow, which contributes to the temperature distribution enhancement. This effect can be visualized through Figure 8, which indicates that the temperature increases from the lower to the upper wall in the channel. The thermophoresis parameter (Nt) is directly related to temperature difference. Figure 9 is an inspection of the temperature

distribution for the variations of Nt. It is evident from Figure 9 that temperature also increases from the lower to the upper wall of the channel as Nt increases. The Prandtl number is related to thermal diffusivity, and from Figure 10, it is evident that the Prandtl number results in enhancing the temperature at the lower wall, whereas the reverse trend is noted at the upper wall of the channel.

Figures 11–16 illustrate the effects of significant parameters for a concentration profile of nanoparticles $\phi(\eta)$ when the power-law index is $n = 1.0$ or $n = 3.0$. It is observed that the power-law index parameter causes a minor change in the behaviour of the concentration profile. Figure 11 demonstrates the influence of the Reynolds number on the concentration profile $\phi(\eta)$. It is clear that
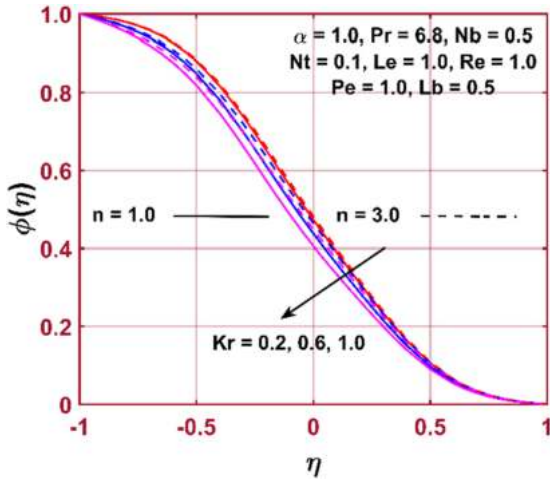
Figure 15: Effect of the chemical reaction parameter (Kr) on $\theta(\eta)$ when the power-law index is $n = 1, 3$.
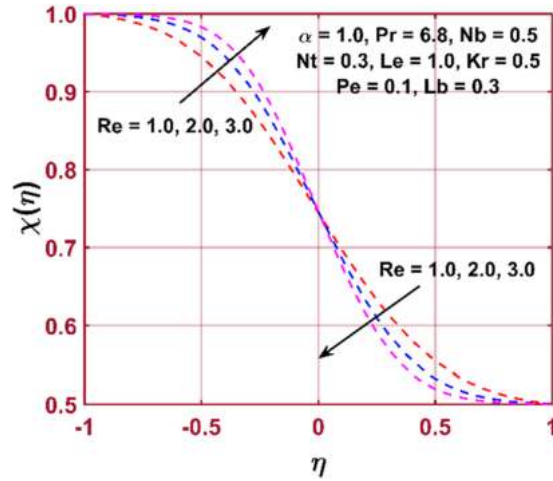

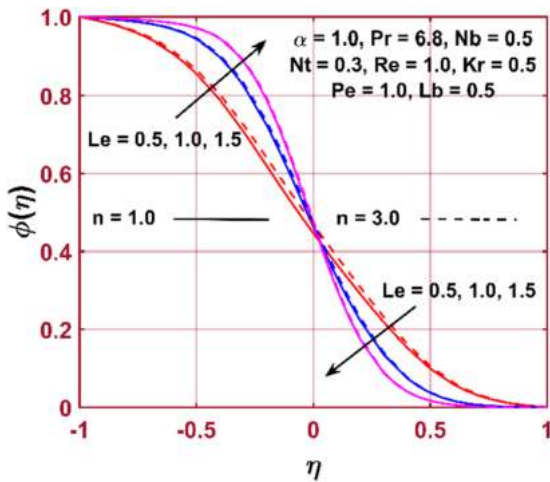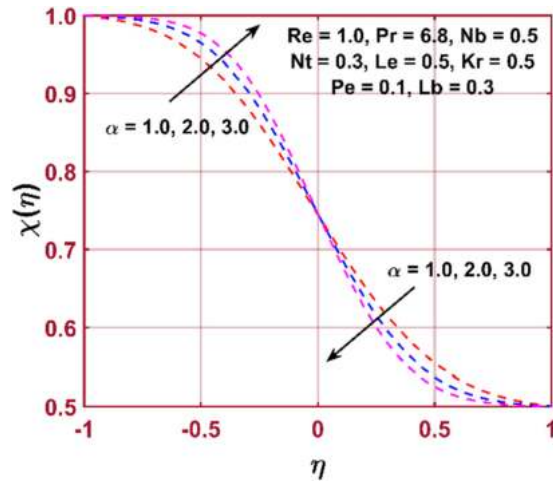**Figure 16:** Effect of the Lewis number (Le) on $\theta(\eta)$ when the power-law index is $n = 1, 3$.

Figure 17: Effect of the Reynolds number (Re) on $\chi(\eta)$.

Figure 18: Effect of the expansion ratio parameter α on $\chi(\eta)$.

Figure 19: Effect of the Péclet number (Pe) on $\chi(\eta)$.

nanoparticle concentration increases at the lower wall but decreases at the upper wall for the power-law index parameter, $n = 1.0$ or $n = 3.0$. The effect of the wall expansion ratio parameter is given in Figure 12, which shows a similar effect to that of the Reynolds number on concentration profile. Figures 13 and 14, respectively, demonstrate the impact of the Brownian motion parameter and the thermophoretic parameter for $n = 1.0$ and $n = 3.0$ on the concentration profile. The nanoparticle concentration increases at the lower wall for both $n = 1$ and $n = 3.0$ with an increase in Nb (Figure 13), while the opposite trend is seen in the case of Nt in Figure 14 and *vice versa*. The impact of the chemical reaction parameter (Kr) is displayed in Figure 15. Kr depends on the nanoparticle concentration and the power-law index. It is
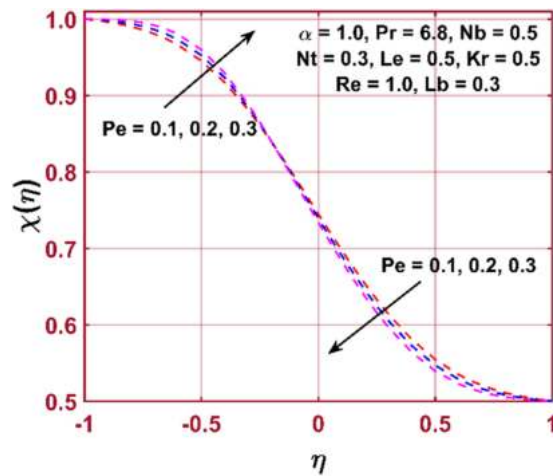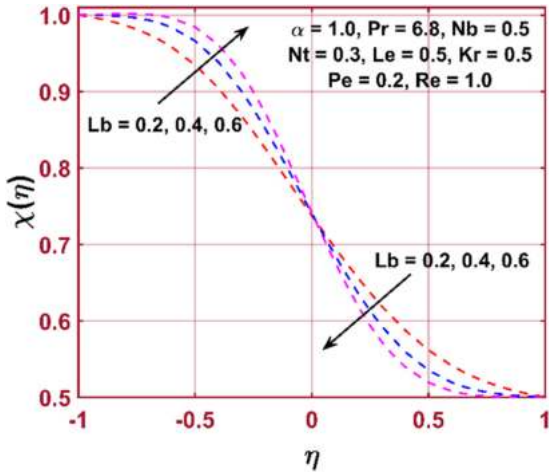
Figure 20: Effect of the bioconvection Lewis number (Lb) on $\chi(\eta)$.

Figure 21: Variation of the local Nusselt number with the Reynolds number.

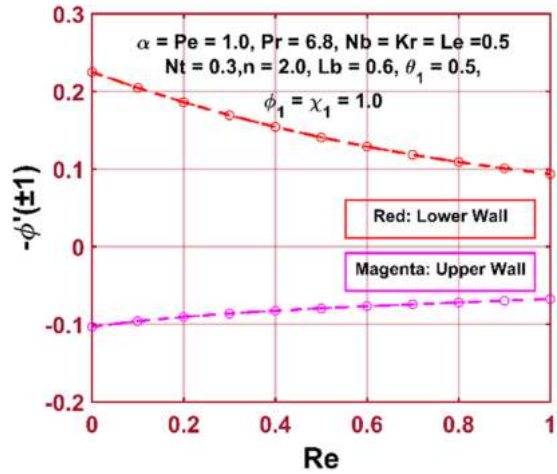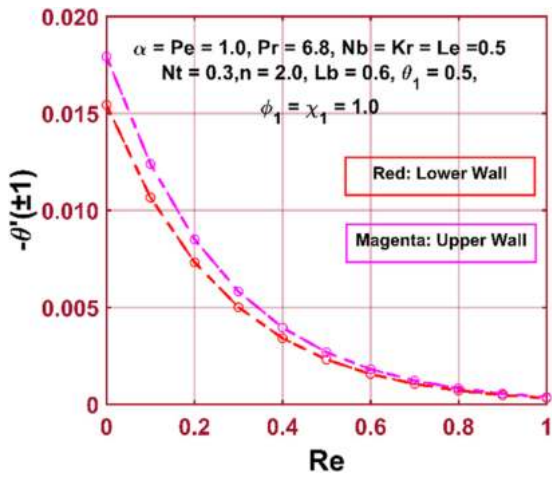**Figure 22:** Variation of the local Nusselt number with the expansion ratio parameter.

Figure 23: Variation of the local Sherwood number with the Reynolds number.

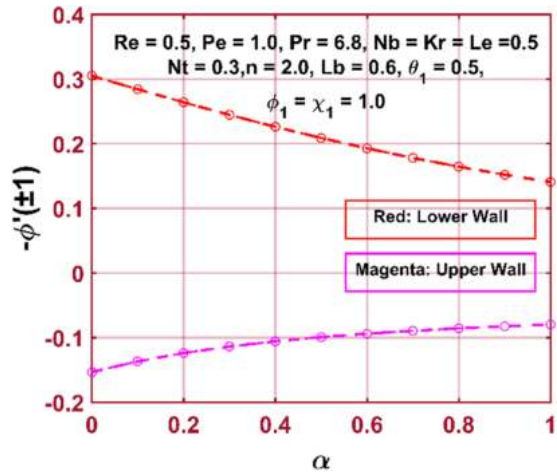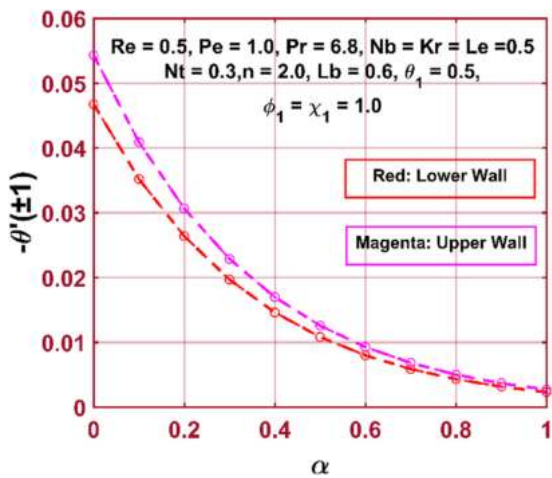**Figure 24:** Variation of the local Sherwood number with the expansion ratio parameter.

evident from Figure 15 that the concentration $\phi(\eta)$ declines as the value of Kr for both $n = 1$ and $n = 3.0$ increases. The effect of the Lewis number is shown in Figure 16. At the lower wall for $n = 1$ and $n = 3.0$, nanoparticle concentration increases with the Lewis number and it is because of the reduction in the mass transfer rate. Hence, the concentration of nanoparticles $\phi(\eta)$ in that region increases. The reverse impact is observed for the upper wall.

Effects of several parameters on density of motile microorganisms $\chi(\eta)$ are demonstrated in Figures 17–20. The Reynolds number (Re) acts in reverse at the lower and upper walls. The microorganisms' density increases at the lower wall due to the increment in Re. The opposite behaviour appears in the case of the upper wall. This
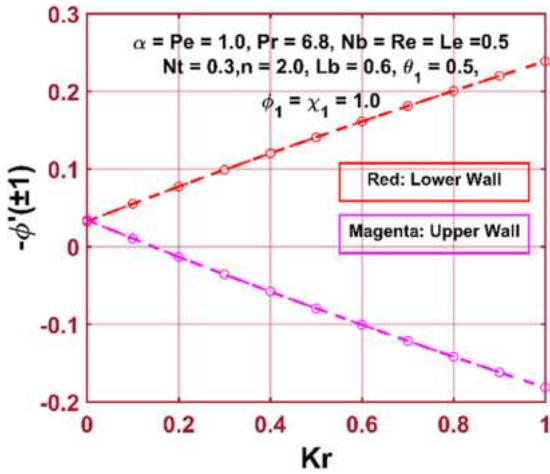
Figure 25: Variation of the local Sherwood number with the chemical reaction parameter.
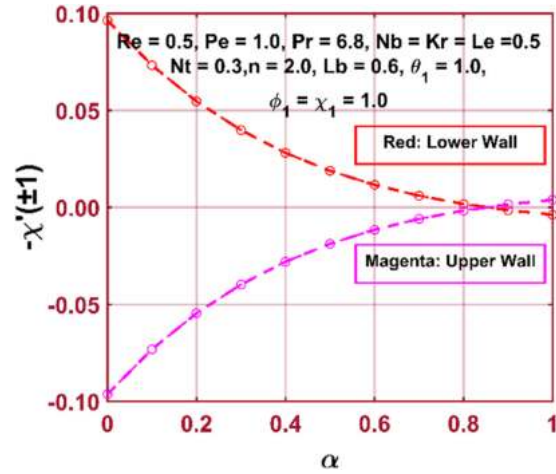

Figure 27: Variation of the motile density number with the expansion ratio parameter.
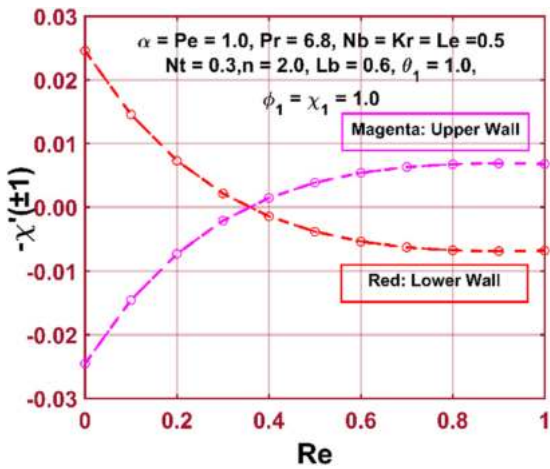

Figure 26: Variation of the motile density number with the Reynolds number.

effect is displayed in Figure 17. Figure 18 shows the contribution of the wall expansion parameter (α) for the motile microorganisms' density. It depicts that $\chi(\eta)$ is an increasing function of α at the lower wall and *vice versa* at the upper wall. The Péclet number is used in calculating the convective heat transfer. The impact of the Péclet number on $\chi(\eta)$ is shown in Figure 19. Due to heat convection at the lower wall, the density of microorganisms increases and decreases at the upper wall. The influence of Lb on $\chi(\eta)$ is presented in Figure 20. Lb depends on diffusion of microorganisms and increases when diffusion of microorganisms decreases. Hence, when Lb increases, $\chi(\eta)$ increases at the lower wall and *vice versa* at the upper wall.

The variation of the local Nusselt number, $-\theta'(\pm 1)$, together with the Reynolds number and the wall expansion ratio parameter is shown in Figures 21 and 22, respectively. The local Nusselt number has positive relationships with both Reynolds number and the wall expansion ratio parameter. Figures 23–25 depict the variation of mass transfer rate $-\phi'(\pm 1)$ at the lower wall as well as the upper wall for the Reynolds number, the wall expansion ratio parameter and the chemical reaction parameter, respectively. The mass transfer rate decreases from the lower to the upper wall of the channel. In Figures 26 and 27, the local density rates of microorganisms, $-\chi'(\pm 1)$, for both lower and upper walls are displayed for Re and α. It is found that at the lower wall, the density rate decreases as Re increases, but this does not occur at the upper wall. Similar impact can be observed for expansion ratio parameter (α).

5 Conclusions and future direction

The main difference between this work and previous is the inclusion of nth order chemical reaction. The present numerical simulation is based on bioconvection of Newtonian nanofluids. The conclusions based on the present investigation are as follows:

- Reynolds number contributes to enhancing the fluid temperature, the concentration of nanoparticles and the density of motile microorganisms at the lower wall. It also has a reciprocal activity at the upper wall of the channel.
- Chemical reaction parameter results in a reduction of the concentration of nanoparticles. Up swimming of microorganisms enhances the concentration of

nanoparticles, and hence concentration increases with an increase in Péclet number.

- Reynolds number has been confirmed as an increasing function of the Nusselt number. However, the Sherwood number and microorganisms' density decrease with the Reynolds number.
- For further research, a hybrid computational technique is required to explore various non-Newtonian nanofluid models in a Jeffery–Hamel flow, namely, the homotopy analysis transform method (Singh et al. [39]).

References

[1] Chakraborty T, Das K, Kundu PK. Framing the impact of external magnetic field on bioconvection of a nanofluid flow containing gyrotactic microorganisms with convective boundary conditions. Alex Eng J. 2018;57:61–71.

[2] Sheikholeslami M. Numerical investigation of MHD nanofluid free convective heat transfer in a porous tilted enclosure. Eng Comput. 2017;34:1939–55.

[3] Freidoonimehr N, Rashidi MM, Momenpour MH, Rashidi S. Analytical approximation of heat and mass transfer in MHD non-Newtonian nanofluid flow over a stretching sheet with convective surface boundary conditions. Int J Biomath. 2017;10:1750008.

[4] Choi SU, Eastman JA. Enhancing thermal conductivity of fluids with nanoparticles. ASME Publ Fed. 1995; 231:99–103.

[5] Abd El-Aziz M. Effects of hall current on the flow and heat transfer of a nanofluid over a stretching sheet with partial slip. Int J Mod Phys C. 2013;24:1350044.

[6] Haq RU, Nadeem S, Khan ZH, Akbar NS. Thermal radiation and slip effects on MHD stagnation point flow of nanofluid over a stretching sheet. Phys E Low Dimens Syst Nanostruct. 2015;65:17–23.

[7] Khanafer K, Vafai K, Lightstone M. Buoyancy-driven heat transfer enhancement in a two-dimensional enclosure utilizing nanofluids. Int J Heat Mass Transf. 2013;46:3639–53.

[8] Tiwari RK, Das MK. Heat transfer augmentation in a two-sided lid-driven differentially heated square cavity utilizing nanofluids. Int J Heat Mass Transf. 2007;50:2002–18.

[9] Buongiorno J. Convective transport in nanofluids. J Heat Trans-T ASME. 2006;128:240–50.

[10] Gupta S, Kumar D, Singh J. MHD mixed convective stagnation point flow and heat transfer of an incompressible nanofluid over an inclined stretching sheet with chemical reaction and radiation. Int J Heat Mass Transf. 2018;118:378–87.

[11] Gupta S, Kumar D, Singh J. Magnetohydrodynamic three-dimensional boundary layer flow and heat transfer of water-driven copper and alumina nanoparticles induced by convective conditions. Int J Mod Phys B. 2019;33:1950307.

[12] Gupta S, Kumar D, Singh J. Analytical study for MHD flow of Williamson nanofluid with the effects of variable thickness, nonlinear thermal radiation and improved Fourier's and Fick's Laws. SN Appl Sci. 2020;2:438.

[13] Zainal NA, Nazar R, Naganthran K, Pop I. Impact of anisotropic slip on the stagnation-point flow past a stretching/shrinking surface of the Al_2O_3-Cu/H_2O hybrid nanofluid. Appl Math Mech-Engl Ed. 2020;41:1401–16.

[14] Naganthran K, Basir MFM, Kasihmuddin MSM, Ahmed SE, Olumide FB, Nazar R. Exploration of dilatant nanofluid effects conveying microorganism utilizing scaling group analysis: FDM Blottner. Phys A. 2020;549:124040.

[15] Bég OA, Uddin MJ, Khan W. Bioconvective non-Newtonian nanofluid transport in porous media containing micro-organisms in a moving free stream. J Mech Med Biol. 2015;15:1550071.

[16] Khan NS, Gul T, Khan MA, Bonyah E, Islam S. Mixed convection in gravity-driven thin film non-Newtonian nanofluids flow with gyrotactic microorganisms. Results Phys. 2017;7:4033–49.

[17] Kumar R, Sood S, Shehzad SA, Sheikholeslami M. Numerical modeling of time-dependent bio-convective stagnation flow of a nanofluid in slip regime. Results Phys. 2017;7:3325–32.

[18] Sokolov A, Goldstein RE, Feldchtein FI, Aranson IS. Enhanced mixing and spatial instability in concentrated bacterial suspensions. Phys Rev E. 2009;80:031903.

[19] Tsai TH, Liou DS, Kuo LS, Chen PH. Rapid mixing between ferro-nanofluid and water in a semi-active Y-type micromixer. Sens Actuators A Phys. 2009;153:267–73.

[20] Kuznetsov A. The onset of thermo-bioconvection in a shallow fluid saturated porous layer heated from below in a suspension of oxytactic microorganisms. Eur J Mech B Fluids. 2006;25:223–33.

[21] Uddin MJ, Kabir M, Bég OA. Computational investigation of Stefan blowing and multiple-slip effects on buoyancy-driven bioconvection nanofluid flow with microorganisms. Int J Heat Mass Transf. 2016;95:116–30.

[22] Aziz A, Khan W, Pop I. Free convection boundary layer flow past a horizontal flat plate embedded in porous medium filled by nanofluid containing gyrotactic microorganisms. Int J Therm Sci. 2012;56:48–57.

[23] Khan WA, Uddin MJ, Ismail AIM. Bioconvective non-Newtonian nanofluid transport over a vertical plate in a porous medium containing microorganisms in a moving free stream. J Porous Media. 2015;18:389–99.

[24] Raees A, Xu H, Sun Q, Pop I. Mixed convection in gravity-driven nano-liquid film containing both nanoparticles and gyrotactic microorganisms. Appl Math Mech-Engl Ed. 2015;36:163–78.

[25] Xun S, Zhao J, Zheng L, Zhang X. Bioconvection in rotating system immersed in nanofluid with temperature dependent viscosity and thermal conductivity. Int J Heat Mass Transf. 2017;111:1001–6.

[26] Naganthran K, Basir MFM, Alharbi SO, Nazar R, Alwatban AM, Tlili I. Stagnation point flow with time-dependent bionanofluid

past a sheet: Richardson extrapolation technique. Processes. 2019;7:722.

[27] Daniel YS, Aziz ZA, Ismail Z, Salah F. Thermal radiation on unsteady electrical MHD flow of nanofluid over stretching sheet with chemical reaction. J King Saud Univ Sci. 2017;31:804–12.

[28] Hayat T, Awais M, Qasim M, Hendi AA. Effects of mass transfer on the stagnation point flow of an upper-convected Maxwell (UCM) fluid. Int J Heat Mass Transf. 2011;54:3777–82.

[29] Hatami M, Sheikholeslami M, Ganji D. Nanofluid flow and heat transfer in an asymmetric porous channel with expanding or contracting wall. J Mol Liq. 2014;195:230–9.

[30] Bég OA, Basir MFM, Uddin M, Ismail AM. Numerical study of slip effects on unsteady asymmetric bioconvective nanofluid flow in a porous microchannel with an expanding/contracting upper wall using Buongiorno's model. J Mech Med Biol. 2017;17:1750059.

[31] Ahmed N, Mohyud-Din ST, Hassan SM. Flow and heat transfer of nanofluid in an asymmetric channel with expanding and contracting walls suspended by carbon nanotubes: A numerical investigation. Aerosp Sci Technol. 2016;48:53–60.

[32] Darvishi M, Khani F, Awad F, Khidir A, Sibanda P. Numerical investigation of the flow of a micropolar fluid through a porous channel with expanding or contracting walls. Propuls Power Res. 2014;3:133–42.

[33] Javanmard M, Taheri M, Abbasi M, Ebrahimi S. Heat transfer analysis of hydromagnetic water–graphene oxide nanofluid flow in the channel with asymmetric forced convection on walls. Chem Eng Res Des. 2018;136:816–24.

[34] Mosayebidorcheh S. Analytical investigation of the micropolar flow through a porous channel with changing walls. J Mol Liq. 2014;196:113–9.

[35] Odelu O, Kumar NN. Slip-flow and heat transfer of chemically reacting micropolar fluid through expanding or contracting walls with Hall and ion slip currents. Ain Shams Eng J. 2018;9:137–47.

[36] Xinhui S, Liancun Z, Xinxin Z, Jianhong Y. Homotopy analysis method for the heat transfer in a asymmetric porous channel with an expanding or contracting wall. Appl Math Model. 2011;35:4321–9.

[37] Kuznetsov A, Nield D. Natural convective boundary-layer flow of a nanofluid past a vertical plate. Int J Therm Sci. 2010;49:243–7.

[38] Gupta S, Kumar D, Singh J. DMP: A maple package for symbolic computation and error estimating to singular two-point boundary value problems with initial conditions. Proc Nat Acad Sci India Sect A. 2019;89:405–14.

[39] Singh J, Rashidi MM, Sushila, Kumar D. A hybrid computational approach for Jeffery–Hamel flow in non-parallel walls. Neural Comput Appl. 2017;31:2407–13.